World Electric Vehicle Journal

MDPI

Article

Research on the Influence of Liquid on Heat Dissipation and Heating Characteristics of Lithium-Ion Battery Thermal Management System

Chuanwei Zhang, Jing Huang *, Weixin Sun, Xusheng Xu and Yikun Li

School of Mechanical Engineering, Xi'an University of Science and Technology, Xi'an 710054, China; zhangcw@xust.edu.cn (C.Z.); 21205224061@stu.xust.edu.cn (W.S.); 21305224004@stu.xust.edu.cn (X.X.); 19205201050@stu.xust.edu.cn (Y.L.)

* Correspondence: 20205224057@stu.xust.edu.cn; Tel.: +86-184-0296-5761

Abstract: A battery thermal management system (BTMS) with functions of heat dissipation and heating by using only one liquid and one structure was studied, and a design for a new type of thermal management device structure was proposed. To find the influence factors of the BTMS on heat dissipation and heating characteristics, we selected and simulated three parameters: inlet size, liquid flow rate, and temperature. The convective heat transfer coefficient h and the Nusselt number Nu were used to analyze the influence of inlet size and liquid velocity on heat transfer intensity. The results show that: (1) In the temperature environment of 298 K with different discharge rates, a pipe diameter of 10 mm is the best size of the BTMS; (2) The increase in flow rate can increase the convective heat transfer coefficient h and the Nusselt number Nu. When the flow rate is 0.02 m/s, the growth rate of h and Nu is the largest; (3) The higher the fluid temperature, the faster the temperature of the battery pack increases in cold environments, but the uneven surface temperature of the battery is also more obvious.

Keywords: liquid cooling; liquid heating; lithium-ion battery; thermal management

Citation: Zhang, C.; Huang, J.; Sun, W.; Xu, X.; Li, Y. Research on the Influence of Liquid on Heat Dissipation and Heating Characteristics of Lithium-Ion Battery Thermal Management System. *World Electr. Veh. J.* **2022**, *13*, 68. https://doi.org/10.3390/wevj13040068

Academic Editor: Michael Fowler

Received: 1 March 2022
Accepted: 13 April 2022
Published: 15 April 2022

1. Introduction

A power battery is one of the main power sources of electric vehicles [1]. It has the advantages of high energy, high-energy density, high power, recyclable use, wide operating temperature range (−30 °C~65 °C), long service life, etc. [2–5]. There are two problems in the use of power batteries: battery performance indicators (specific energy, specific power, driving range, charging capacity, etc.) do not meet the requirements, and the battery management system is not perfect [6]. Due to the uneven surface temperature of the power battery during use, there is a significant difference in the maximum temperature difference between the battery surface during 1C discharge and 2C discharge [7]. Therefore, if there is no suitable BTMS, the temperature problem of the power battery mentioned above during use will be more significant [8,9], the battery performance will be relatively reduced [10], and thermal runaway may also occur [11]. The commonly used scheme of BTMS is to use air, phase change materials, heat pipes, liquids, and other materials to raise or lower the temperature of the outer surface of the battery [12]. The above BTMS schemes all have advantages and disadvantages. Due to the large side surface area of the battery, it provides advantages for the liquid-based heat dissipation contact area, which can lead to more effective overall heat transfer performance [13]. Du et al. [14] experimentally studied a microchannel cooling system for battery cooling, and every single battery would be in contact with six micro-channels. Compared with the natural condition of discharge in a battery without cooling, the average temperature of the battery is reduced by 43.7% and 47.3% at 1C and 1.5C, respectively. Huo et al. [15] established a three-dimensional thermal

management model and studied the influence of the number of coolant channels on the battery temperature. The research results indicate that more cooling channels have an increased thermal performance. Therefore, the use of liquid thermal management is a good choice.

Liquid-cooled-based BTMS, referred to as LC-BTMS, is the most reliable type of heat exchange method used in lithium-ion batteries for pure electric vehicles in recent years. It can be divided into two types: conventional type and micro-scale type. Conventional LC-BTMS can be divided into indirect cooling LC-BTMS and direct cooling LC-BTMS [16]. However, although liquid thermal management can increase the contact area with the battery, direct contact with the liquid can easily cause the battery to short circuit. Therefore, choosing indirect contact with the battery through the device is a common method currently used by researchers [17]. For example, Chen et al. [18] compared the thermal performance of four cooling strategies: forced air cooling, fin cooling, indirect liquid cooling, and direct liquid cooling, and found that the power consumption required for air cooling is 2~3 of other methods. Compared with direct cooling, indirect cooling is a better choice. Tesla pure electric vehicles use 1:1 glycol/water solution as the cooling medium for Models' on-board LC-BTMS and have carried out a new structural design and supporting maintenance strategies to meet the requirements, making Tesla Pure electric vehicles widely praised by the market and favored by consumers.

At present, the liquid is often used as a cooling medium in thermal management systems, while another medium is used for heating. This not only increases the power consumption of the battery and increases energy consumption but also reduces the electricity efficiency of electric vehicles. For example, Yiran Zheng et al. [19] used the method of combining liquid and composite PCM in the state of high-rate discharge to only dissipate heat to the battery. The main heat dissipation method is liquid cooling, while the composite phase change material removes the thermal opacity in the battery pack. Area, providing relatively little heat absorption. Chuanwei Zhang et al. [20] designed a cooling arrangement design, using liquid and heat pipes to well control thermal runaway, and using thermoelectric fins when heating the battery pack. Therefore, this subject decided to use the same liquid medium to conduct thermal management research on electric vehicle power batteries. In thermal management, thermal conductivity, temperature, and flow rate are the keys to heating and cooling the battery. We established a three-dimensional model of the thermal management device, analyzed the influence of different inlet sizes and different inlet flow rates on the temperature difference and pressure difference, and used the convective heat transfer coefficient h and Nusselt number Nu for quantitative analysis. Investigated the effect of heat flow in BTMS at low temperature on batteries. Different from existing work, we have the following innovations:

(1) Designed a new liquid-based thermal management system structure, which has a larger surface area directly in contact with the battery, has more effective overall heat transfer, and provides an experimental carrier for thermal management research;
(2) At present, liquids are often used as coolants, referred to as "liquid cooling". This research not only uses water to cool down but also uses hot water to heat the battery when the battery is in a low-temperature environment. Raise the surface temperature of the battery to a suitable operating temperature range;
(3) Using the same structure and same liquid realizes the balance of the battery's working temperature, saves the redundant structure, reduces the weight of the whole vehicle, and improves the energy utilization rate.

2. Theoretical Analysis

A commercial lithium-ion battery ($LiFePO_4$) is used in this article, the specific parameters are shown in Table 1.

Table 1. Parameter table of lithium-ion battery.

Serial Number	Parameter Name		Numerical Value
1	Standard capacity		72 (Ah)
2	Rated voltage		3.2 (V)
3	Charging (constant current and constant voltage CC-CV)	Maximum charging current	1 (C)
		Charging upper limit voltage	3.65 (V)
4	Discharge at room temperature	Maximum continuous discharge current	2 (C)
		End of discharge voltage	2.5 (V)
5	Operating temperature	Discharge	−5~50 (°C)
		Charge	−20~50 (°C)
6	Weight		1.78 (kg)
7	Cycle life		≥3000 cycle
8	Shell material		aluminum

As can be seen in the table, the charging temperature of $LiFePO_4$ battery is −20~50 °C, and the discharging temperature is −5~50 °C. The maximum continuous discharge current rate is 2C, so we can study the temperature change of the battery under the discharge rate of 0.5C, 1.0C, 1.5C, and 2C.

3. Numerical Simulations

3.1. Model of BTMS

As shown in Figure 1, the battery thermal management model contains five single batteries. To place the BTMS and battery smoothly, an external box is designed, which contains five cells. The two large sides of each cell are touched by hollow aluminum plates. This design increases the contact area. Due to the influence of the acceleration of gravity g, the upper part of the aluminum plate is designed as a water inlet, and the lower part is designed as a water outlet. In order to prevent liquid leakage, each water inlet and outlet are connected with a larger diameter water pipe outside the box. The overall size of the BTMS is 268 mm × 260 mm × 230 mm, and the size of the cell is 135 mm × 30 mm × 220.8 mm. The size of the hollow aluminum plate is shown in Table 2. The inlet size 'd' is optional. The change of inlet size 'd' will change the hollow area inside the aluminum plate.

To simplify the physics problem, make the following assumptions:

(1) The liquid flowing through the pipe is an incompressible Newtonian fluid.
(2) Thermal properties of all materials are constant.
(3) In the simulation process, assuming that the physical properties of the battery are uniform, the average specific heat capacity of the battery cells is applied.
(4) Thermal contact resistance is not considered.

3.2. Simulation Model Design

3.2.1. Model Thermogenesis Analysis

Studies have shown [21] that the total heat Q generated by lithium batteries during charging and discharging is mainly composed of four types: Reaction heat Q_r, Polarization heat Q_p, Heat of side reaction Q_s. Among them, the heat generated by the side reaction heat is very small and can be ignored [22]. Therefore, the total heat release can be expressed as:

$$Q = Q_r + Q_j + Q_p \tag{1}$$

The heating power per unit volume of the battery is:

$$q = \frac{Q}{V} = \frac{I^2 R_{OR}}{V} \tag{2}$$

where q is the body heat source of the single battery, I is the charge and discharge current of the battery, R_{OR} is the ohmic internal resistance of the battery, and V is the volume of the single battery.

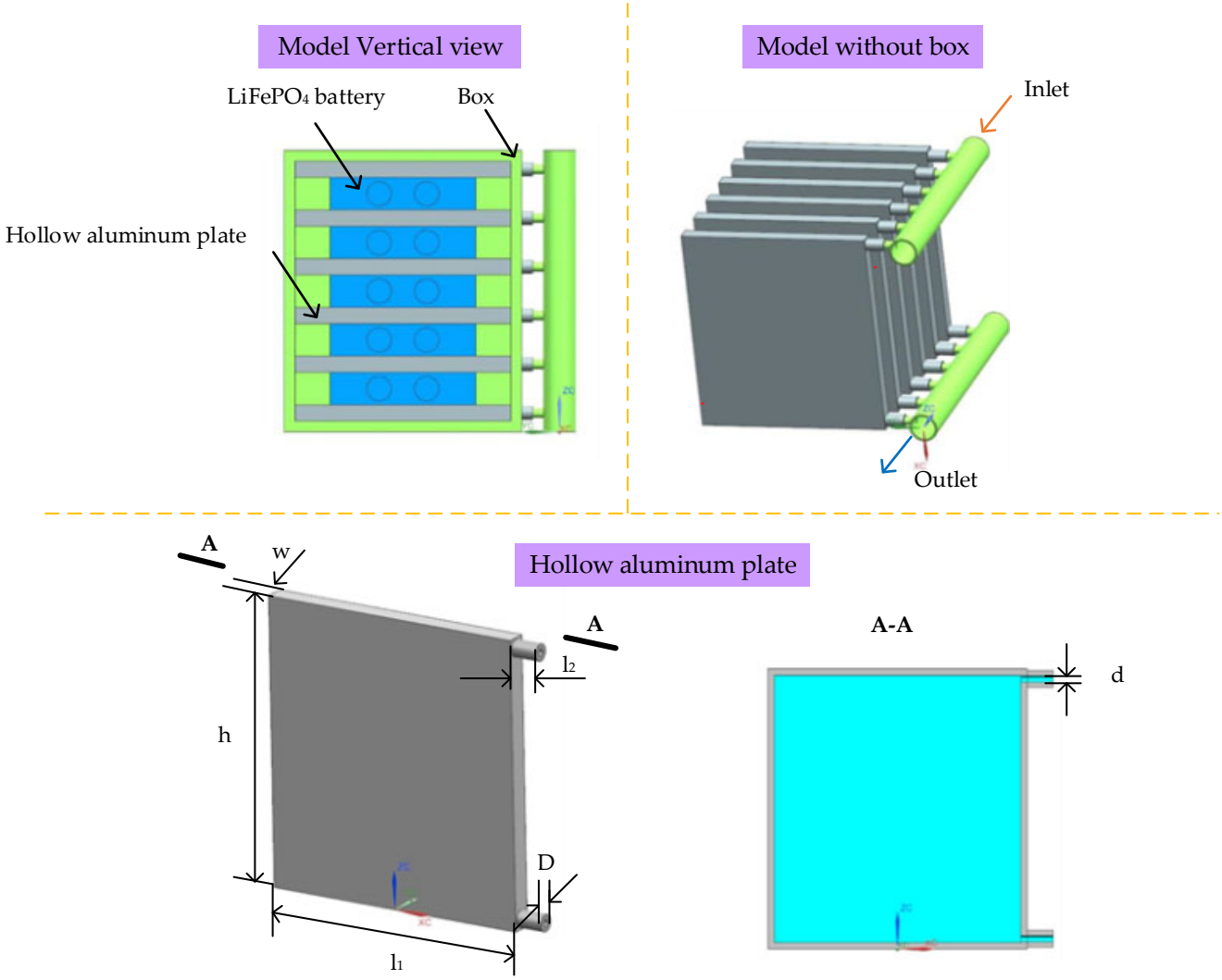

Figure 1. Battery thermal management system model.

Table 2. The size of hollow aluminum plate.

Parameter	l_1	w	h	D	l_2	d
Size (mm)	200	15	215	15	20	Optional

The heat generation power, internal heat, and discharge time of a $LiFePO_4$ battery at different discharge rates can be obtained, as shown in Table 3. Furthermore, the discharge time can be used to simulate battery parameters under different discharge rates.

Table 3. Battery discharge characteristics.

Discharge Rate (C)	0.5	1	1.5	2
Discharge Current (A)	36	72	108	144
Heat Production Power (W)	1.23	4.925	11.08	19.7
Internal Heat (W/m^3)	1376	5507	12,391	22,029
Discharge Time (s)	7200	3600	2400	1800

3.2.2. Simulation Model Design

The convective heat transfer coefficient h is defined by:

$$h = 0.023\frac{\lambda_w}{D}\left(\frac{D\vec{v}\rho_l}{\mu}\right)^{0.8}\left(\frac{C_{pl}\mu}{\lambda_w}\right)^{n} \quad (3)$$

where D is the pipe diameter, m. λ_w is the thermal conductivity of fluid, W/(m·K); $\vec{v}$ is the velocity vector of the fluid, m/s; ρ_l is the density of the fluid, kg/m^3; $c_{\rho l}$ is the heat capacity of the fluid, J/(kg·K); μ is the dynamic viscosity of fluid, m^2/s.

When the fluid is heated, n = 0.4; when it is cooled, n = 0.3.

The Nu number (Nusselt number) is an important parameter that can be used to judge the intensity of convection in convective heat transfer:

$$N_u = \frac{h \bullet D}{\lambda_w} \quad (4)$$

The energy conservation equation, continuous equation, and momentum conservation equation are given as follows:

$$\begin{cases} \frac{\partial \rho_l}{\partial t} + \nabla \bullet (\rho_l \vec{v}) = 0 \\ \frac{\partial}{\partial t}(\rho_l \vec{v}) + \nabla \bullet (\rho_l \vec{v}\vec{v}) = -\nabla p \\ \frac{\partial}{\partial t}(\rho_l c_{pl} t_l) \nabla \bullet (\rho_l c_{pl} \vec{v} t_l) = \nabla \bullet (\lambda_w \nabla t_l) \end{cases} \quad (5)$$

where t_l is the temperature of the fluid, K.

The Reynolds number (Re) is defined by:

$$R_e = \frac{D\vec{v}\rho_l}{\mu} \quad (6)$$

The flow of the fluid through the channel is calculated as turbulent flow (the Reynolds number is greater than 2300).

The fluid passed into the pipeline is deionized water, and the physical parameters are shown in Table 4.

Table 4. Fluid parameters.

Material	Density (kg/m^3)	Specific Heat Capacity (J/(kg·k))	Thermal Conductivity (W/(m·K))
Deionized water	998.2	4182	0.6

3.2.3. Boundary Conditions and Initial Conditions

The initial management of the entire system is set to 298 K. The heat transfer coefficient of natural convection between the wall of the pack and the outside is set to 5 W/(m^2·K) [23,24]. The internal heat of the battery is set according to different discharge rates. According to different experimental conditions, for example, the speed of the pipe inlet is set to 0.02 m/s, the initial temperature is set to 298 K, the pipe outlet pressure is standard atmospheric pressure, and other parameters are maintained as a default.

3.2.4. Grid Independence Verification

The model with an inlet size of 5 mm was selected as the experimental object for grid independence verification, and six thermal management models with different grid numbers were verified with Fluent 20.0. The number of grids is compared: 413,792, 513,742, 684,884, 778,326, and 953,749. The result of grid verification is shown in Figure 2. When the number of grids tends to 684,884, the highest temperature of the

entire system tends to stabilize; 684,884 was selected as the grid number of the BTMS model in this paper.

3.3. Model Verification

The thermal management device is placed in a constant temperature and humidity box, with an ambient temperature of 298 K and a humidity of 0%, and the convective heat transfer coefficient of the environment is 5 W/(m^2·K). Set the battery pack discharge rate to 1C, that is, set the discharge current to 72 A, and set the simulation duration to 3600 s in the simulation. The battery temperature collection points are shown in Figure 3a. T-type thermocouples are used to paste three points on the surface of the battery. The T-type thermocouples are connected to the Agilent digital logger, which can accurately transmit data to the computer. The measured points are the positive electrode area, negative electrode area, and middle area. As shown in Figure 3b, the temperatures of the three points are different. The temperature of the positive electrode area is the highest, followed by the negative electrode area, and the lowest temperature is the middle area. Therefore, we use the average temperature of three points to compare with the simulation, as shown in Figure 3c. The results show that there is a gap between the data and the simulation at the beginning of the experiment. The reason may be that the thermocouple connector installed on the surface of the battery exchanges heat with the air, which leads to temperature errors. In addition, the temperature of the laboratory environment may also affect the experimental results [25–27]. The experimental results are consistent with the numerical results, and the maximum temperature difference between the experimental and simulation results is 0.5 K. In short, the battery thermal management simulation model is accurate enough to research the heat performance of BTMS.

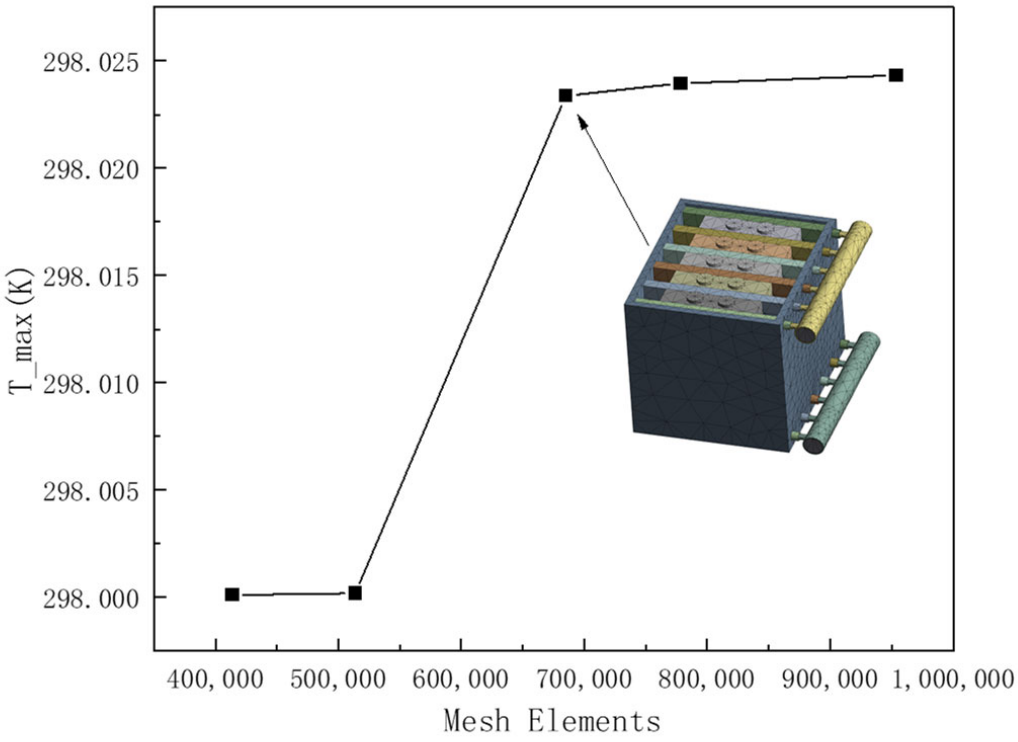

Figure 2. Grid independence verification.

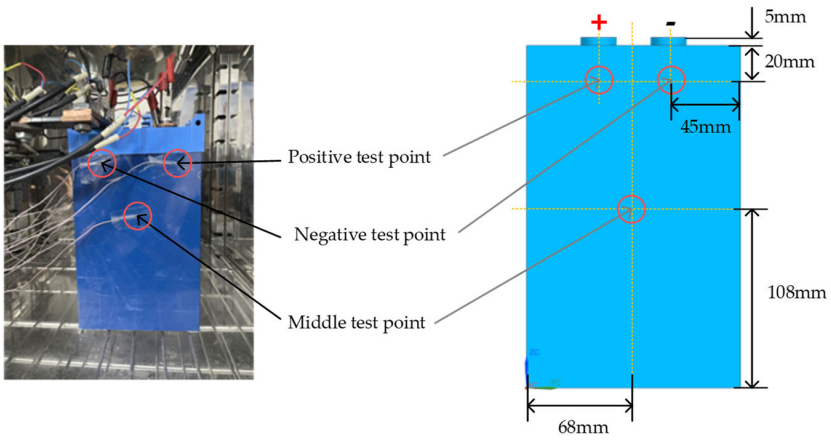

(**a**)

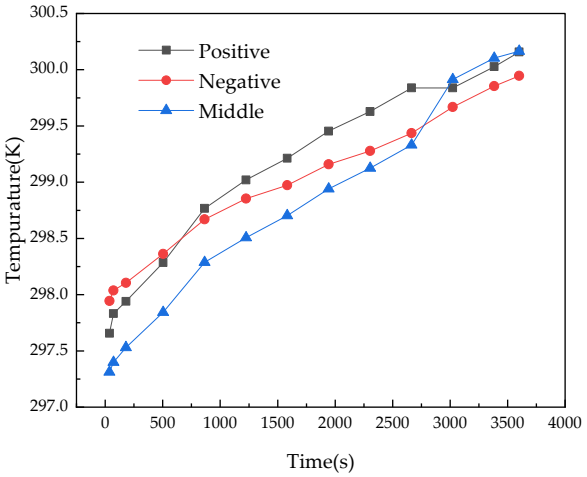

(**b**)

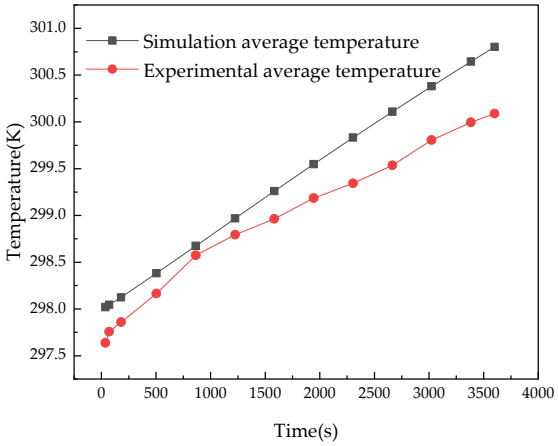

(**c**)

Figure 3. Cell experimental verification. (**a**) The location of the three points of battery temperature measurement. (**b**) The temperature at three points of 1C discharge. (**c**) Comparison of experimental and simulation results.

4. Analytical Methods

Inlet sizes, flow rates, heating temperature, and time all affect the temperature control performance of liquid BTMS, so we need to determine the best parameter combination for each other [28]. Quantitative analysis is performed using convective heat transfer coefficient h and Nusselt number Nu.

4.1. Inlet Size Selection

To research the influence of inlet size on the thermal performance of BTMS, we first set the inlet flow rate to be constant, which is selected as 0.02 m/s. The diameters of the aluminum plate inlet and outlet are 5 mm, 8 mm, 10 mm, and 12 mm. Observe the temperature difference on the surface of the battery and the pressure difference on the inlet of the BTMS.

4.2. Flow rate Selection

Similar to the method of 4.1, the inlet size is fixed, and the optimal inlet size in the previous analysis is selected. The liquid with a flow rate of 0.01~0.1 m/s [29] is selected to pass through the inlet, and the temperature change and pressure difference change are observed.

4.3. Fluid Temperature Selected on BTMS Heating

After the inlet size and flow rate are determined, the BTMS also has the function of heating the battery pack in a cold environment that is not suitable for working. It can be seen from Table 1 that the charging temperature of the $LiFePO_4$ battery used in the experiment is 253~323 K, and the discharging temperature is 268~323 K. Therefore, we choose to simulate BTMS heating to 298 K before battery discharging in a low-temperature environment of 253 K. To research the relationship between required fluid temperature and time for the heating to 298 K, the temperature of the incoming fluid is selected: 298 K, 303 K, 308 K, 313 K, 318 K, 323 K.

5. Results and Discussion

Before analyzing the influence of inlet size, flow rate, and liquid temperature on the BTMS, we first simulated the discharge state of the battery in a natural environment at 298 K without BTMS interference. The maximum average temperature and maximum temperature difference of discharge are shown in Figure 4. The results show that the maximum temperature of the battery surface(T_max) and the temperature difference between the battery pack(T_differ) increase with the increase in the discharge rate. When the discharge rate is 2C, the T_max is 314.2 K, and the T_differ is 16 K, which is completely outside the range of the maximum temperature difference allowed for the normal operation of the battery. Therefore, it is necessary to manage the temperature of batteries.

5.1. The Influence of Inlet Size on Thermal Performance of BTMS

As the inlet size of the hollow aluminum plate increases, the ability of the battery module to conduct heat outward also be improved. This is because the variation of pipe diameter increases the fluid flow area, reduces the wall thickness of the fluid in contact with the outside, and increases the heat transfer strength. The fluid is allowed by the larger contact area between BTMS and the battery to take away more of the heat generated by the battery, resulting in improved cooling efficiency. As shown in Figure 5a, is the maximum temperature graph when the pipe diameter is 5 mm, 8 mm, 10 mm, 12 mm, and the battery is discharged at different charge rates. The graph shows that although the pipe diameters are different, they can all achieve the purpose of cooling the battery. This is because when we set different rates of discharge in the simulation, the discharge time is different, and the time length of the BTMS working time is also different correspondingly. It can also be seen from Figure 5a that the average temperature of the

battery at 12 mm, is 0.5C is higher than the average temperature of other discharge rates. It can be seen that the pipe diameter of 12 mm can not control the stability of the surface temperature of the battery.

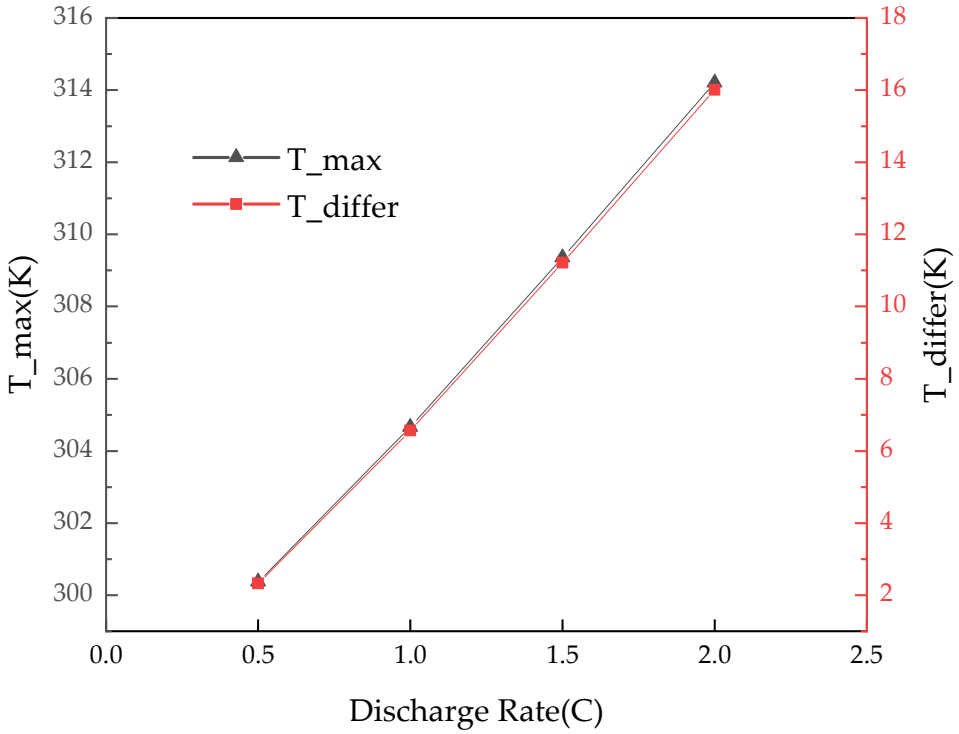

Figure 4. Battery discharge temperature at 298 K.

Therefore, to compare the effect of different pipe diameters on the temperature of the BTMS more effectively, we made the temperature difference and pressure difference curves of different pipe diameters, as shown in Figure 5b. It can be seen that when the inlet size is 5 mm, the smaller part of the pipeline receives the largest pressure, and the pressure difference reaches 35.3703 Pa, which will damage the pipe, so the 5 mm pipe is not practical. According to the temperature difference curve, it can be seen that when the inlet size is 12 mm, the temperature difference of the battery reaches the maximum, which is not conducive to equalizing the temperature of the battery.

To analyze these data more effectively, the convective heat transfer coefficient h and the Nusselt number Nu were selected for quantitative analysis. As shown in Figure 6, the convective heat transfer coefficient of the BTMS decreases as the inlet size increases. When the inlet size is 5 mm to 12 mm, the convective heat transfer coefficient h is reduced from 196.327 $W \cdot m^{-2} \cdot K^{-1}$ As small as 164.792 $W \cdot m^{-2} \cdot K^{-1}$. The Nusselt number Nu increased from 1.636 to 3.296. This is because the increase in pipe diameter increases the contact area between the liquid and the aluminum plate. Although the overall convective heat transfer coefficient of the BTMS decreases with the increase in pipe diameter, the Nu growth rate curve shows that the overall heat transfer intensity of the BTMS is increasing. This shows that the increase in inlet size improves the ability of the battery module to conduct heat to the outside.

After the above comparison, we found that the difference between 8 mm and 10 mm diameter is not obvious. Therefore, for better selection, we set the initial temperature of the battery to the temperature after the 2C discharge state and then cool the battery by passing liquid through the BTMS. It was found that, as shown in Figure 7a, when the maximum temperature of the battery was reduced to 298 K, the time required for a pipe diameter of 8 mm was 459.7 s, while as shown in Figure 7b, the time required for a 10 mm pipe was 280.5 s, which shows that the cooling time of the BTMS with a diameter of 10 mm is shorter

than that of 8 mm. From this, it can be judged that in order to achieve faster and better thermal management, the diameter of 10 mm is the best.

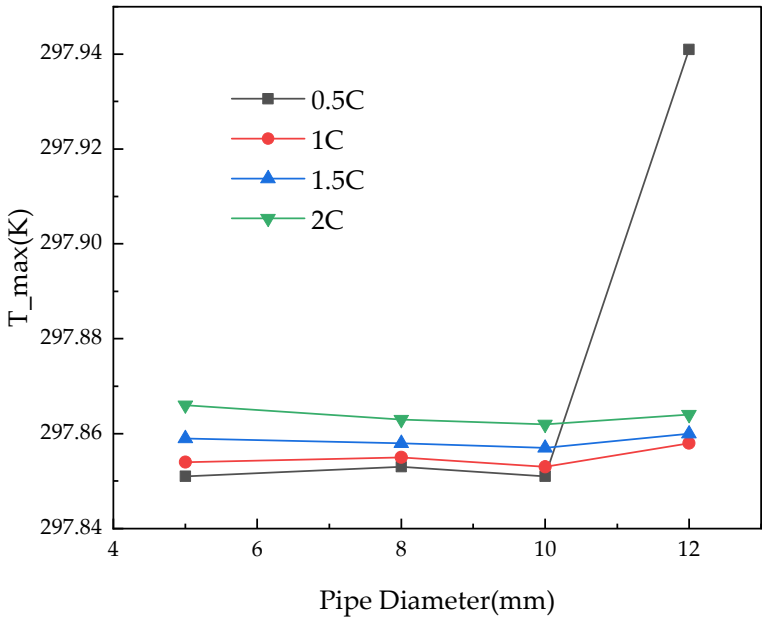

(**a**)

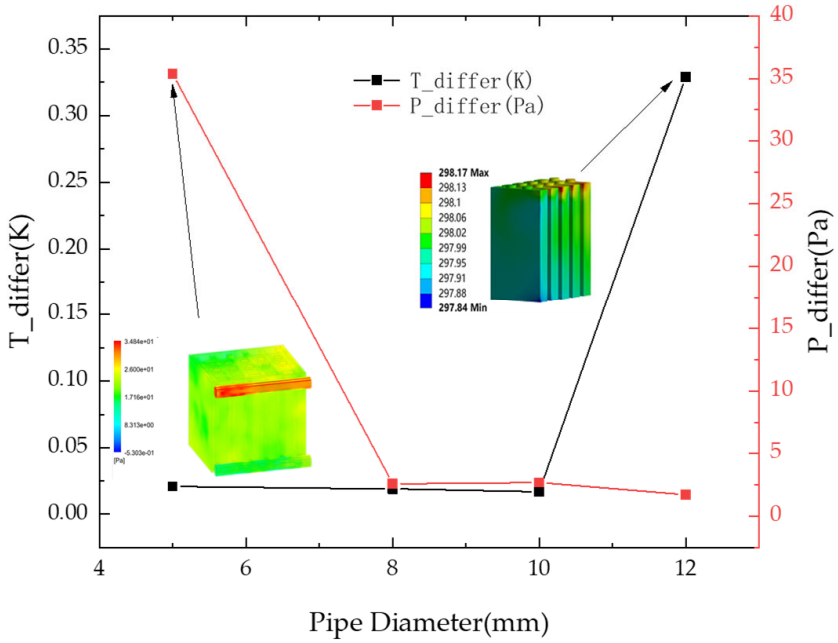

(**b**)

Figure 5. The influence of inlet size on thermal performance of BTMS. (**a**) Maximum temperature curve of the battery. (**b**) Effect of inlet size on temperature difference and pressure difference.

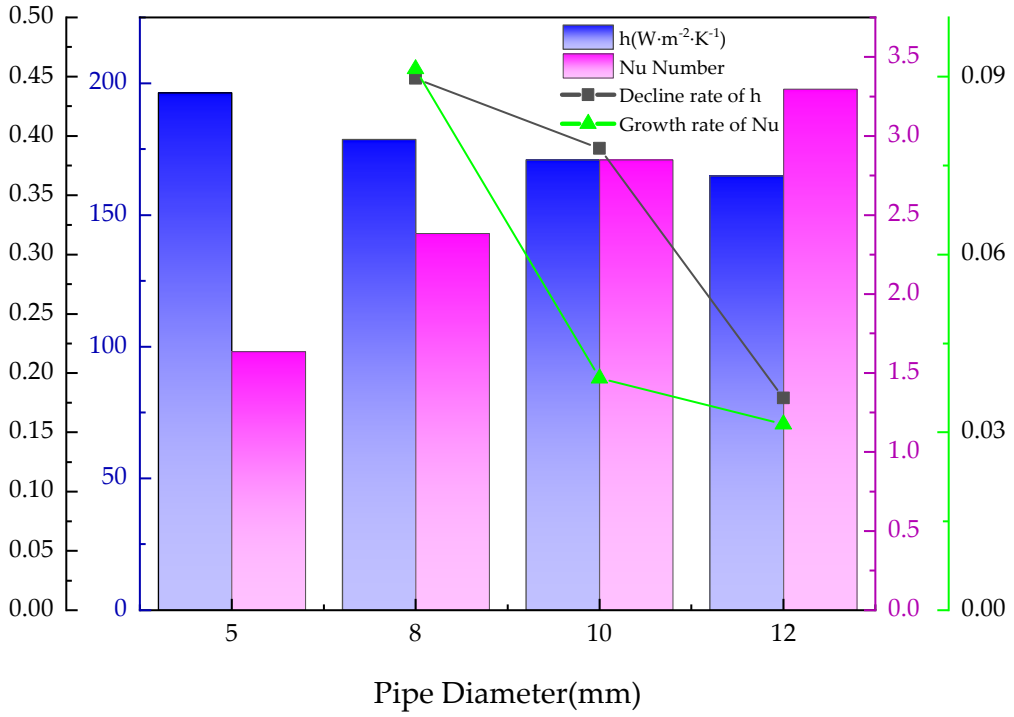

Figure 6. Effect of inlet size on h and Nu.

5.2. The Influence of Flow Rate on Thermal Performance of BTMS

According to the results in Section 5.1, the optimal diameter of the selected pipe is 10 mm. As shown in Figure 5a, the temperature change of the battery is most obvious when the battery is discharged at 2C. Therefore, the 2C discharge rate is selected. As shown in Figure 8, the pressure difference gradually increases as the flow rate increases. The research found that when the flow rate is 0.01 m/s, the temperature difference at the end of the battery discharge is 0.022 K; when the flow rate is 0.02 m/s to 0.08 m/s, the temperature difference is 0.017 K, but when the flow rate is 0.1 m/s, the battery surface temperature difference reaches 4.278 K. This is because when the flow rate increases to a certain level, for the BTMS, the liquid flowing through the aluminum plate has less contact time with the aluminum plate wall, and the liquid cooling efficiency is low. When the flow rate is 0.1 m/s, the pressure difference reaches 44.249 Pa, which is seriously beyond the capacity of THE BTMS structure, resulting in leakage phenomenon and even battery short circuit accidents. This shows that the flow velocity of 0.1 m/s cannot be selected.

Similarly, two criterion numbers, the convective heat transfer coefficient h and the Nusselt number Nu, will be used to analyze and discuss. As shown in Figure 9, as the flow velocity increases, both the convective heat transfer coefficient h and Nu gradually increase, and the convective heat transfer coefficient increases from 97.981 $W \cdot m^{-2} \cdot K^{-1}$ to 618.216 $W \cdot m^{-2} \cdot K^{-1}$, Nu Number increased from 1.633 to 10.304. This is because when the flow rate increases, the coolant flow into the BTMS also increases, enhancing the heat transfer intensity of the BTMS. According to the growth rate curve of h and Nu, it is found that when the flow velocity is 0.02 m/s, the growth rate of both reaches the highest. Therefore, for this BTMS, 0.02 m/s is the optimal flow rate.

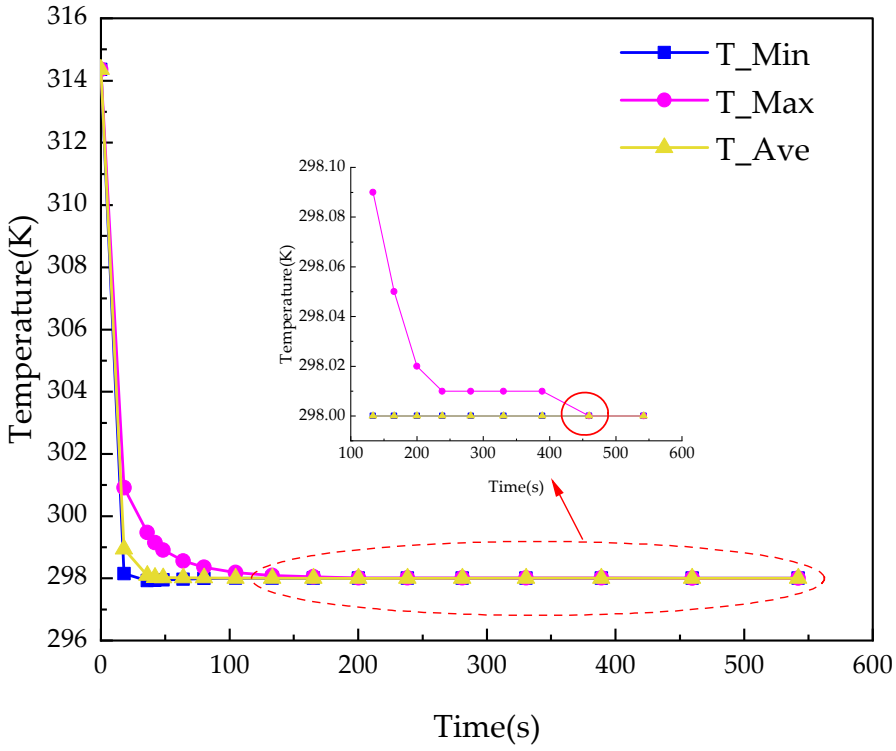

(**a**)

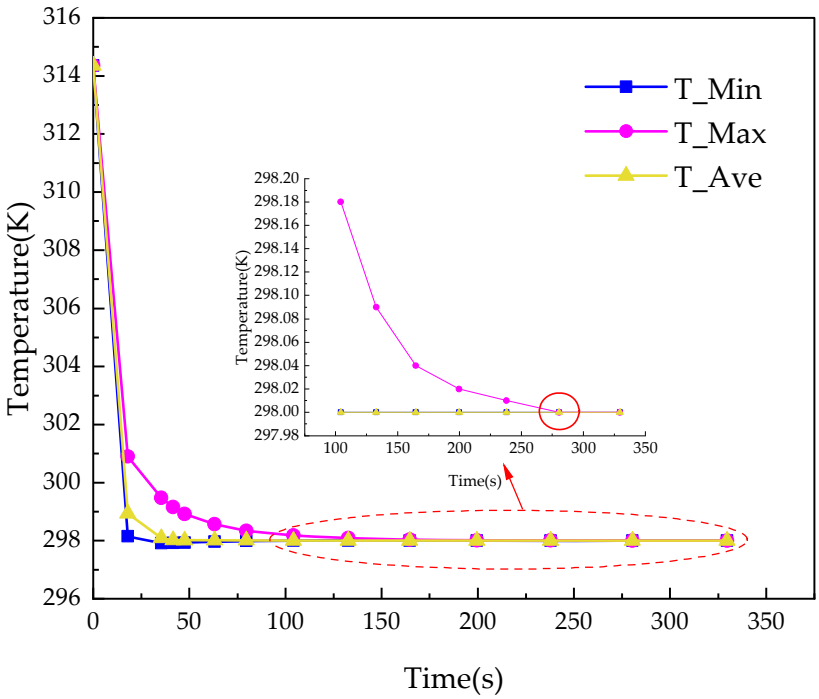

(**b**)

Figure 7. Comparison of cooling time between 8 mm and 10 mm. (**a**) 8 mm diameter cooling time. (**b**) 10 mm diameter cooling time.

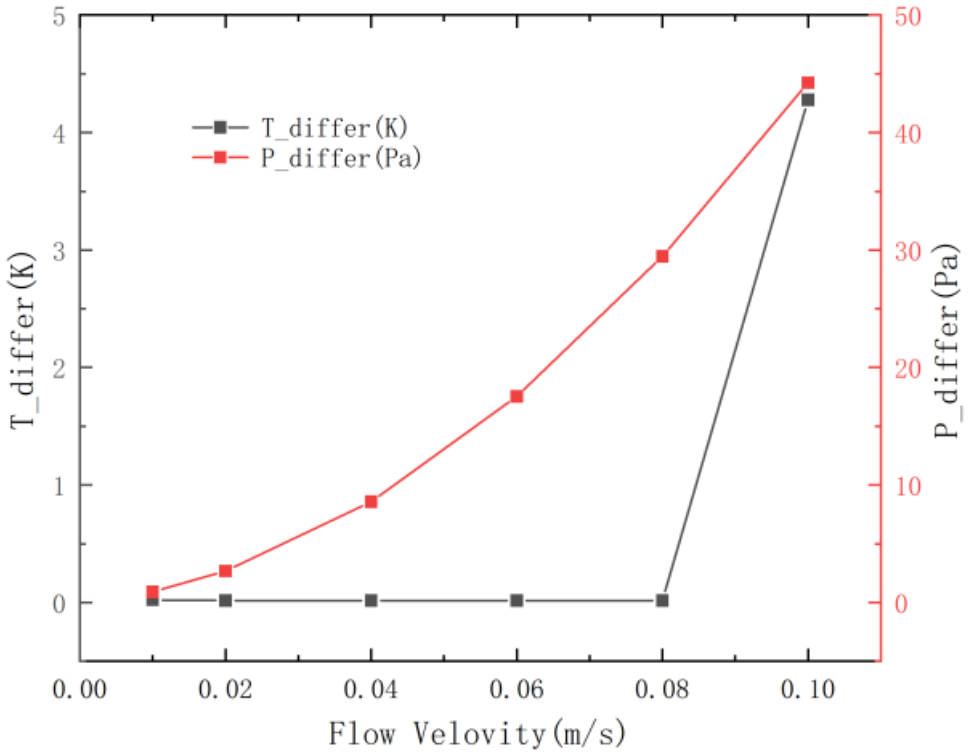

Figure 8. Effect of flow rate on the temperature difference and pressure difference.

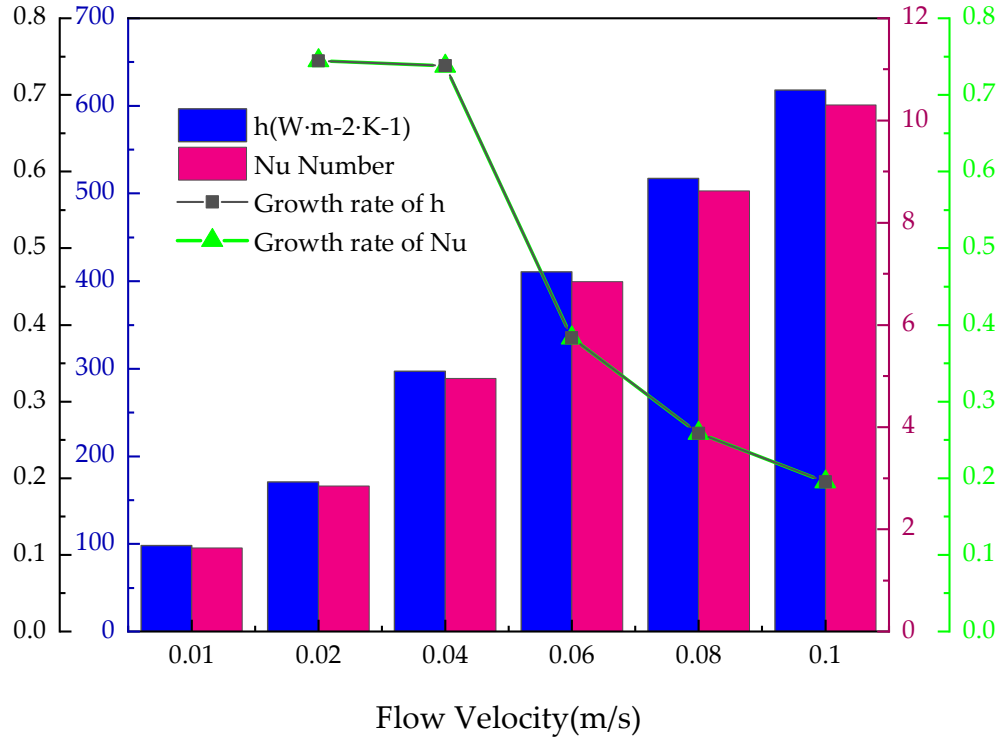

Figure 9. Effect of flow velocity on h and Nu.

Therefore, we also find that in fluid-based BTMS, the flow rate of fluid should be lower. This ensures that the BTMS does not break under too much pressure and allows the fluid flowing into the BTMS to spend more time in indirect contact with the battery, bringing in or taking away more heat.

5.3. The Influence of Fluid Temperature on BTMS Heating

According to the results of Sections 5.1 and 5.2, the BTMS works best when the inlet size is 10 mm, and the flow velocity is 0.02 m/s. In a low-temperature environment of 253 K, when the temperature of the incoming fluid is 298 K, 303 K, 308 K, 313 K, 318 K, 323 K, the time required to reach 298 K is simulated and analyzed. As shown in Figure 10, it shows that the duration of 323 K is the shortest, only 2.31 s. However, the size of the temperature difference increases as the temperature of the incoming fluid increases. At 323 K, the temperature difference of the single-cell reached 20.72 K. Because the battery temperature difference needs to be controlled within 5 K [30], only when the fluid temperature was 298 K and 303 K did the maximum temperature difference remain below 5 K. However, hot water at 303 K takes at least ten times less time to heat the battery to 298 K (room temperature) than water at 298 K.

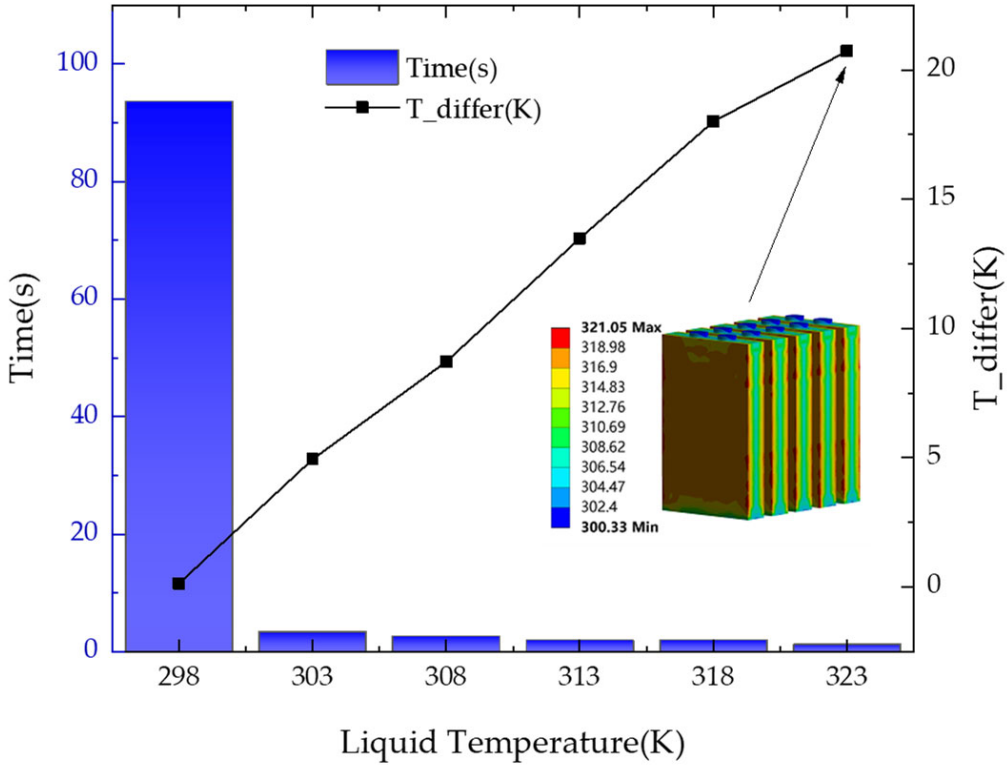

Figure 10. The influence of fluid temperature on BTMS.

When the BTMS heats the battery pack, shortening the heating time so that the battery can start working as soon as possible is a point to consider. The appropriate temperature is also an important selection point; otherwise, the temperature will be too high, negatively impacting the battery.

6. Conclusions

At present, due to oil shortages and environmental pollution, new energy vehicles have gradually replaced traditional fuel vehicles, and battery management systems are becoming more and more important. Based on the commercial $LiFePO_4$ battery, this research has developed a liquid BTMS to study heat dissipation and heating. Related parameters: the influence of inlet size, flow rate, and liquid temperature on the performance of the BTMS are analyzed. The convective heat transfer coefficients h and Nu are used to quantitatively analyze the parameters. The main conclusions of this article are as follows:

(1) A 10 mm pipe diameter is the optimal size for this BTMS. The increase in pipe inlet size improves the ability of the battery module to transmit heat to the outside, reduces the wall thickness of fluid contact with the outside, and the BTMS has

a large surface area in direct contact with the battery, which further increases the heat transfer intensity. At the same time, the temperature of the battery pack is better balanced, and the T_differ is controlled within 1 K when the battery is discharged at different discharge rates.

(2) The greater the liquid flow rate, the greater the BTMS pressure difference; the temperature difference tends to be stable, and can be controlled within 5 K. In this paper, when the flow velocity is 0.02 m/s, the growth rates of h and Nu are the largest. In addition, liquid-based BTMS flow rates are recommended to be smaller. This can avoid the damage to the BTMS structure caused by excessive pressure and can also increase the heat exchange time of the liquid, thereby bringing or taking away more heat.

(3) High-temperature fluid can quickly increase the temperature of the battery pack in a cold environment, but it will also cause the uneven surface temperature of the battery, and the higher the fluid temperature, the more obvious this phenomenon is. Therefore, if it needs to heat the battery quickly, a high-temperature fluid can be introduced first, and after the battery reaches the desired temperature, a lower-temperature fluid can be used to maintain it.

Author Contributions: Conceptualization, C.Z. and J.H.; methodology, C.Z. and J.H.; software, J.H.; validation, J.H. and W.S.; formal analysis, J.H.; investigation, C.Z.; resources, C.Z.; data curation, X.X.; writing—original draft preparation, J.H.; writing—review and editing, J.H., W.S. and X.X.; visualization, Y.L.; supervision, C.Z.; project administration, C.Z.; funding acquisition, C.Z. All authors have read and agreed to the published version of the manuscript.

Funding: This research was funded by the National Natural Science Foundation of China: Research on the Integrated Control Method of the Lateral Stability of Distributed Drive Mining Electric Vehicles (51974229), The 2021 Youth Innovation Team Construction Scientific Research Program of Shaanxi Provincial Education Department (Project No.: 21JP071) and Shaanxi Province Innovation Talent Promotion Plan-Science and Technology Innovation Team Project: 2021TD-27.

Institutional Review Board Statement: Not applicable.

Informed Consent Statement: Not applicable.

Data Availability Statement: Not applicable.

Conflicts of Interest: The authors declare no conflict of interest.

References

1. Widmaier, M. Influence of carbon distribution on the electrochemical performance and stability of lithium titanate based energy storage devices. *J. Electrochim. Acta* **2017**, *247*, 1006–1018. [CrossRef]
2. Whittingham, M.S. Materials challenges facing electrical energy storage. *MRS Bull.* **2008**, *33*, 411–419. [CrossRef]
3. Pistoia, G. *Lithium-Ion Batteries: Advances and Applications*; Newnes; Elsevier: Amsterdam, The Netherlands, 2013.
4. Nitta, N.; Wu, F.; Lee, J.T.; Yushin, G. Li-ion battery materials: Present and future. *Mater. Today* **2015**, *18*, 252–264. [CrossRef]
5. Andwari, A.M.; Pesiridis, A.; Rajoo, S.; Martinez-Botas, R.; Esfahanian, V. A review of Battery Electric Vehicle technology and readiness levels. *Renew. Sustain. Energy Rev.* **2017**, *78*, 414–430. [CrossRef]
6. Hannan, M.A.; Lipu, M.S.H.; Hussain, A.; Mohamed, A. A review of lithium-ion battery state of charge estimation and management system in electric vehicle applications: Challenges and recommendations. *Renew. Sustain. Energy Rev.* **2017**, *78*, 834–854. [CrossRef]
7. Chen, S. Research on Thermal Management System of Power Battery. Master's Thesis, Xi'an University of Science and Technology, Xi'an, China, 2020.
8. Shim, J.; Kostecki, R.; Richardson, T.; Song, X.; Striebel, K.A. Electrochemical analysis for cycle performance and capacity fading of a lithium-ion battery cycled at elevated temperature. *J. Power Sources* **2002**, *112*, 222–230. [CrossRef]
9. Amine, K.; Liu, J.; Belharouak, I. High-temperature storage and cycling of C-LiFePO4/graphite Li-ion cells. *Electrochem. Commun.* **2005**, *7*, 669–673. [CrossRef]
10. Bandhauer, T.M.; Garimella, S.; Fuller, T.F. A critical review of thermal issues in lithium-ion batteries. *J. Electrochem. Soc.* **2011**, *158*, R1. [CrossRef]
11. Wang, Q.; Ping, P.; Zhao, X.; Chu, G.; Sun, J.; Chen, C. Thermal runaway caused fire and explosion of lithium ion battery. *J. Power Sources* **2012**, *208*, 210–224. [CrossRef]

12. Patel, J.R.; Rathod, M.K. Recent developments in the passive and hybrid thermal management techniques of lithium-ion batteries. *J. Power Sources* **2020**, *480*, 228820. [CrossRef]
13. Jarrett, A.; Kim, I.Y. Design optimization of electric vehicle battery cooling plates for thermal performance. *J. Power Source* **2011**, *196*, 10359–10368. [CrossRef]
14. Du, X.; Qian, Z.; Chen, Z.; Rao, Z. Experimental investigation on mini-channel cooling–based thermal management for Li-ion battery module under different cooling schemes. *Int. J. Energy Res.* **2018**, *42*, 2781–2788. [CrossRef]
15. Huo, Y.; Rao, Z.; Liu, X.; Zhao, J. Investigation of power battery thermal management by using mini-channel cold plate. *Energy Convers. Manag.* **2015**, *89*, 387–395. [CrossRef]
16. Nagasubramanian, G. Electrical characteristics of 18650 Li-ion cells at low temperatures. *J. Appl. Electrochem.* **2001**, *31*, 99–104. [CrossRef]
17. Pesaran, A.; Santhanagopalan, S.; Kim, G.H. *Addressing the Impact of Temperature Extremes on Large format Li-Ion Batteries for Vehicle Applications (Presentation)*; Office of Scientific & Technical Information Technical Reports; National Renewable Energy Lab: Golden, CO, USA, 2013; Volume 38, pp. 3797–3806.
18. Chen, K.; Li, X. Accurate Determination of Battery Discharge Characteristics-a Comparison between Two Battery Temperature Control Methods. *J. Power Sources* **2014**, *247*, 961–966. [CrossRef]
19. Zheng, Y.; Shi, Y.; Huang, Y. Optimisation with adiabatic interlayers for liquid-dominated cooling system on fast charging battery pack. *Appl. Therm. Eng.* **2019**, *147*, 636–646. [CrossRef]
20. Zhang, C.; Xia, Z. A Coolant Circulation Cooling System Combining Aluminum Plates and Copper Rods for Li-Ion Battery Pack. *Energies* **2020**, *13*, 4296. [CrossRef]
21. Noboru, S. Thermal behavior analysis of lithium-ion batteries for electric and hybrid vehicles. *J. Power Sources* **2001**, *99*, 70–77.
22. Jiang, C. Research of Thermal Characteristics of Battery Pack in Pure Electric Vehicle. Master's Thesis, Hefei University of Technology, Hefei, China, 2015.
23. Liu, W.; Jia, Z.; Luo, Y.; Xie, W.; Deng, T. Experimental investigation on thermal management of cylindrical Li-ion battery pack based on vapor chamber combined with fin structure. *Appl. Therm. Eng.* **2019**, *162*, 114272. [CrossRef]
24. Chen, K.; Hou, J.; Song, M.; Wang, S.; Wu, W.; Zhang, Y. Design of battery thermal management system based on phase change material and heat pipe. *Appl. Therm. Eng.* **2021**, *188*, 116665. [CrossRef]
25. Yang, T.; Yang, N.; Zhang, X.; Li, G. Investigation of the thermal performance of axial-flow air cooling for the lithium-ion battery pack. *Int. J. Therm. Sci.* **2016**, *108*, 132–144. [CrossRef]
26. Chen, F.; Huang, R.; Wang, C.; Yu, X.; Liu, H.; Wu, Q.; Qian, K.; Bhagat, R. Air and PCM cooling for battery thermal management considering battery cycle life. *Appl. Therm. Eng.* **2020**, *173*, 115–154. [CrossRef]
27. Javani, N. Heat transfer and thermal management with PCMs in a Li-ion battery cell for electric vehicles. *Int. J. Heat Mass Transf.* **2014**, *72*, 72–690. [CrossRef]
28. Jiaqiang, E. Orthogonal experimental design of liquid-cooling structure on the cooling effect of a liquid-cooled battery thermal management system. *Appl. Therm. Eng.* **2018**, *132*, 508–520. [CrossRef]
29. Yi, F. Effects analysis on heat dissipation characteristics of lithium-ion battery thermal management system under the synergism of phase change material and liquid cooling method. *Renew. Energy* **2022**, *181*, 472–489. [CrossRef]
30. Pesaran, A.A. Battery thermal models for hybrid vehicle simulations. *J. Power Sources* **2002**, *110*, 377–382. [CrossRef]